

Liquid Phase Epitaxy growth of Tm3+-doped CaF2 thin-films based on LiF solvent

Gurvan Brasse, Pavel Loiko, C. Grygiel, Philippe Leprince, Abdelmjid Benayad, Franck Lemarié, Jean-Louis Doualan, Alain Braud, Patrice Camy

▶ **To cite this version:**

Gurvan Brasse, Pavel Loiko, C. Grygiel, Philippe Leprince, Abdelmjid Benayad, et al.. Liquid Phase Epitaxy growth of Tm3+-doped CaF2 thin-films based on LiF solvent. Journal of Alloys and Compounds, 2019, 803, pp.442-449. 10.1016/j.jallcom.2019.06.288 . hal-02887852

HAL Id: hal-02887852

https://normandie-univ.hal.science/hal-02887852

Submitted on 25 Oct 2021

HAL is a multi-disciplinary open access archive for the deposit and dissemination of scientific research documents, whether they are published or not. The documents may come from teaching and research institutions in France or abroad, or from public or private research centers.

L'archive ouverte pluridisciplinaire **HAL**, est destinée au dépôt et à la diffusion de documents scientifiques de niveau recherche, publiés ou non, émanant des établissements d'enseignement et de recherche français ou étrangers, des laboratoires publics ou privés.



Distributed under a Creative Commons Attribution - NonCommercial 4.0 International License

Version of Record: https://www.sciencedirect.com/science/article/pii/S0925838819323795
Manuscript_3cd81ae02369b80e48612edc422aebb3

Liquid Phase Epitaxy growth of Tm^{3+}-doped CaF_2 thin-films based on LiF solvent

Gurvan Brasse*, Pavel Loiko, Clara Grygiel, Philippe Leprince, Abdelmjid Benayad, Franck Lemarie, Jean-Louis Doualan, Alain Braud, and Patrice Camy

Centre de recherche sur les Ions, les Matériaux et la Photonique (CIMAP), UMR 6252 Normandie University, ENSICAEN, UNICAEN, CEA, CNRS, 14000 Caen, France

**Corresponding author, e-mail: gurvan.brasse@ensicaen.fr*

ABSTRACT: Single-crystalline Tm^{3+}-doped calcium fluoride (Tm^{3+}:CaF_2) films were grown onto (100) oriented undoped bulk CaF_2 substrates by Liquid Phase Epitaxy method using LiF as a solvent. The growth was performed at the temperatures of 853–865 °C. Crack-free transparent films with a high doping concentration of ~6 at.% and a thickness up to ~100 μm were obtained. The film structure and morphology were characterized by confocal microscopy, X-ray diffraction and scanning electron microscopy. High resolution X-ray diffraction and reciprocal space mapping confirmed the high crystallinity and the low mosaicity of the films. Energy-Dispersive X-ray spectroscopy revealed a uniform distribution of Tm^{3+} ions in the films. The Tm^{3+}:CaF_2 films exhibit a broadband emission at ~2 μm and are of interest for waveguide lasers. The use of CaF_2-LiF binary system is also promising for fabrication of other rare-earth-doped CaF_2 layers.

Keywords: liquid phase epitaxy; Calcium fluoride; Thin films; Thulium ions; Luminescence.

© 2019 published by Elsevier. This manuscript is made available under the CC BY NC user license
https://creativecommons.org/licenses/by-nc/4.0/

1. Introduction

Liquid Phase Epitaxy (LPE) is a well-known method to produce single-crystalline thin films of high optical quality [1,2]. It is a flux method, where a solvent is used to decrease the growth temperature of the solute. The first LPE results about materials for optical applications were reported for cubic garnets [3]. Since then, LPE has been applied to a variety of crystal hosts with different symmetries, e.g., cubic $Y_3Al_5O_{12}$ [4], tetragonal $LiYF_4$ [5] or monoclinic $KY(WO_4)_2$ [6]. During the LPE process, a uniform μm-thick crystalline film is grown on flat polished single-crystalline surface along the desired crystallographic direction [1].

LPE-grown crystalline thin films doped with trivalent rare-earth ions (RE^{3+}) are attractive for laser applications. Under certain conditions, they can exhibit a positive refractive index contrast with respect to the substrate (e.g., simply due to the introduction of active ions [7] or passive (buffer) ones [8] or due to a compositional disorder of the film [9]) resulting in light confinement via total internal refraction. This leads to waveguide laser applications of such films [10-12]. The latter can also be implemented in microchip [13] or thin-disk [14] lasers and amplifiers.

Among the results reporting the LPE growth of crystalline thin-films for optical applications, just few of them concern fluorides. However, RE^{3+}-doped fluoride crystals are very suitable for laser applications especially in the near-mid-infrared spectral range, thanks to a broad transparency range, low refractive index, low phonon energies, good thermo-mechanical properties and the ability to accommodate various RE^{3+} ions showing attractive spectroscopic properties. To date, most of the studies concerning the LPE growth of fluorides focused on $LiYF_4$ [5,8] and few reports exist also on CaF_2 [15,16].

Calcium fluoride (CaF_2) is a well-known *bulk* material for fabrication of optical components such as lenses or windows. This is due to its broadband transparency (0.13–10 μm), low refractive index ($n \approx 1.43$) [17], as well as good thermal and thermo-mechanical properties, namely high thermal conductivity (~9.7 W/mK) [18]. CaF_2 is also attractive because it can be doped with the RE^{3+} ions which substitute the Ca^{2+} ones in the crystal structure [19,20], while a charge compensation occurs to compensate the valence difference between ions. Moreover, CaF_2 can be easily grown by the Czochralski (Cz) method [21], as well as by the Bridgman method.

There exist multiple studies dedicated to the fabrication of undoped crystalline CaF_2 thin films by using various techniques such as molecular beam epitaxy (MBE) [22], electron beam evaporation (EBE) [23], thermal evaporation [24], R.F. magnetron sputtering [25] or pulsed laser deposition (PLD) [26] typically on silicon (Si) substrates. This is because of the very close lattice parameters of CaF_2 and Si, that allows the use of CaF_2 as a buffer layer for further deposition steps. CaF_2 films doped with Er^{3+} [27], Yb^{3+} [28] and Pr^{3+} [29] ions were already grown by the MBE method and their optical and spectroscopic properties were studied, suggesting the positive refractive index difference with respect to the substrate which is needed for waveguiding applications.

In [15,16], CaF_2 films doped with Yb^{3+} and Tm^{3+} ions were produced by LPE on CaF_2 substrates using $CaCl_2$ as a solvent. $CaCl_2$ allows the growth of RE^{3+}:CaF_2 films in a

temperature range from 820 to 875 °C, depending on the molar ratio of CaF_2 / $CaCl_2$. Nevertheless, this solvent is a hygroscopic salt that is also corrosive for the metallic equipment that constitutes the LPE setup. $CaCl_2$ is also volatile at these working temperatures and can coat the inner walls of the chamber within a short time (after few days of experiments).

From these considerations, we aimed to demonstrate the LPE growth of high optical quality single-crystalline Tm^{3+}:CaF_2 thin films by using another solvent, namely LiF, which is very promising for further development of LPE-based RE^{3+}-doped CaF_2 micro-structures.

Thulium (Tm^{3+}) ions have been selected because of their intense and broadband emission in CaF_2 crystals, which is located in the eye-safe spectral range around 2 μm related to the $^3F_4 \rightarrow {}^3H_6$ transition. Tm lasers are of high interest for medicine, spectroscopy and environmental sensing [28]. Moreover, the Tm^{3+}:CaF_2 crystals have been already recognized as suitable gain media for ~2 μm lasers [20,29].

2. Liquid Phase Epitaxy growth

For the LPE growth, lithium fluoride (LiF) was used as a solvent to crystallize Tm^{3+}-doped CaF_2 films onto nominally pure (undoped) CaF_2 substrate at temperatures lower than the melting point of CaF_2 (~1418 °C) [21]. Indeed, according to the phase diagram of the CaF_2–LiF binary system [30] shown in Fig. 1, CaF_2 can be grown from a molten solution at temperatures lower than 900 °C. Working at the lowest possible temperature is better to avoid the damage of the experimental setup and to limit the vaporization of the solvent and thus the evolution of the chemical composition of the bath of molten raw materials. A molar composition of (65% LiF – 30% CaF_2 – 5% TmF_3) was chosen corresponding to an expected growth temperature of about 850 °C. The molar ratio of TmF_3 was fixed to be 5 mol% which corresponds to an atomic ratio of 14.3 at.% with respect to Ca. Thulium was introduced in the form of TmF_3 which was achieved by fluorination of Tm_2O_3 precursor (purity: 4N). The oxide reagent (Tm_2O_3) presents a better purity and is cheaper than TmF_3. The purity of the other used raw materials was 99.5% for CaF_2 and >99.5% for LiF.

The experimental LPE setup is shown in Fig. 2. It consists of a two-zone vertical tubular furnace and a quartz tube used as a growth chamber. A glassy carbon crucible is placed in the zone of the furnace that presents the lowest vertical temperature gradient between the bottom and the surface of the molten bath. The fluorides at the molten state are very reactive with oxygen and moisture to form oxyfluoride compounds that affect the optical quality of the RE^{3+}:CaF_2 films and modify their spectroscopic properties [31]. For this purpose, the sealed chamber has to be in a good secondary vacuum state (pressure: ~10^{-6} mbar) and then to be refilled with Argon gas.

First, the raw materials were weighted according to the molar composition and they were mixed to achieve a homogeneous powder. The crucible containing the batch was then introduced into the growth chamber. When a proper vacuum was reached, the crucible was heated up to 900 °C (above the melting temperature of the mixture) and kept at this temperature during several hours (h); a good homogenization of the melt was obtained thanks to a mechanical stirring. Then, the temperature was decreased to be close to the theoretical

saturation temperature of ~850 °C. The experimental growth temperature was determined empirically by diving test substrates in the molten bath. The substrates used were cut from high optical grade undoped CaF_2 wafers (CRYSTRAN, Ltd), which were extracted from undoped bulk CaF_2 crystals grown by using the Czochlalski (Cz) method. The substrates were oriented such that the [100] crystallographic axis was orthogonal to their surface. They had a thickness of 2.0 mm with a lateral size of ~10×30 mm^2. Both surfaces of the substrates were polished with a measured surface roughness in the nm-scale (see Section 4.1), as the epitaxy process and the crystalline quality of the Tm^{3+}:CaF_2 films strongly depend on this parameter. After have been cleaned, the prepared substrates were dived vertically in the molten bath and rotated at a rate of 10 revolutions per minute (r.p.m.). After completing the growth, the sample was slowly removed from the flux and cooled down to room temperature (~20 °C). No post-growth annealing was applied to the layers.

An overview of the fabrication process of single-crystalline Tm^{3+}:CaF_2 layers grown onto oriented CaF_2 substrates is shown in Fig. 3. In our experiments, crack-free transparent Tm^{3+}:CaF_2 films were obtained over a broad temperature range between 853 °C and 865 °C for growth durations between 20 and 60 min. These temperatures are lower than in the previous study [16] where Tm^{3+}:CaF_2 films were grown by the LPE method using $CaCl_2$ as a solvent. The measured thickness of the as-grown films t was in the range 20–120 μm with a growth rate of 0.5–2.0 μm/min, depending on the growth temperature and duration. The observed film thicknesses are larger than in the previous work (t = 5 μm) [16]. For further characterizations, the edge surface of the epitaxies was also polished.

3. Experimental

The surface morphology of the as-grown Tm^{3+}:CaF_2 films was studied in reflection mode by using a confocal optical microscope (model Sensofar S-neox) equipped with a blue light-emitting diode (LED, 405 nm). To characterize the surface roughness of the substrates, the same microscope was used in an interferometric mode in the manner to reach the nm-range resolution.

The polished side surface of the epitaxy was observed by using an inversed optical polarized microscope (OPTIKA, model XDS-3MET) equipped with a white lamp as an illumination source. The observation of the layer / substrate interface was facilitated by the refractive index contrast between them and allowed for the thickness measurement of the grown films.

The high resolution X-ray diffraction (XRD) patterns were measured with a Bruker AXS D8 Discover diffractometer using a four-circle goniometer, a line focus Cu X-ray source equipped with a Goebel mirror and a Ge (220) double-bounce monochromator providing a parallel and monochromatic (Cu $K_{\alpha 1}$ radiation, λ = 0.15406 nm) incident X-ray beam. A Ge (220) crystal analyzer was also used to further limit the scintillator detector acceptance. Symmetric 2θ-θ scans and reciprocal space maps (RSM) obtained by taking a series of 2θ-ω patterns (±0.5° around the reference) at successive ω values (ω = θ ± Δ; ±0.5° around the reference) were recorded. For the RSM representation, the DxTools viewer [32] was used.

For the EDX compositional analysis, a scanning electron microscope (SEM, Jeol 6400) was used. It was equipped with a tungsten filament thermoelectronic gun and a 10 mm² X-microanalysis diode (Oxford-instrument).

The Tm^{3+} ions in the films were excited with a continuous-wave Ti:Sapphire laser (model 3900S, Spectra Physics) tuned to ~760 nm. The pump radiation was focused on the sample using a spherical lens (f = 50 mm) and the luminescence was collected with another lens and an optical fiber. The spectra were measured using an optical spectrum analyzer (OSA, model AQ6375B, Yokogawa) with a resolution of 0.1 nm. The spectral sensitivity of the detection system (OSA + fiber) was calibrated using a broadband lamp.

4. Results and discussion

4.1. Morphology of the films

The sample described in this Section was produced at a growth temperature of 854 °C for 45 min. Very similar morphology was observed on other samples. A picture of the substrate and of the as-grown Tm^{3+}:CaF_2 / CaF_2 epitaxy is shown in Fig. 4. The epitaxial layer is crack-free, translucent and colorless. The white edge of the grown film is due to the remaining LiF solvent.

The confocal microscope images of the top surface of the as-grown Tm^{3+}:CaF_2 film captured with the magnifications of 10× and 100× are shown in Fig. 5. The surface is smooth but not perfectly flat. Its morphology looks like a hilly landscape in the μm-scale. This can be explained by thermo-dynamical considerations: the surface energy of a curved surface is less than that of a perfectly flat one. As a result, the growth front takes the more stable configuration at the atomic scale during the LPE process. The central part of the film is free of parasitic solvent crystallization.

A 3D-topography of the as-grown Tm^{3+}:CaF_2 film surface is achieved by using the confocal microscope. Then a 2D-transverse profile along the (AB) cut is extracted and presented in Fig. 6(a). By this way, the root-mean-square (RMS) roughness is measured to be less than 1 μm, while the transverse width of the hills on the surface is about 10 μm. For comparison, we also observed the polished undoped CaF_2 substrate, by using the microscope in an interferometric configuration, Fig. 6(b), and the measured RMS surface roughness was below 2 nm.

Microscope images of the polished end-facet of the Tm^{3+}:CaF_2 / CaF_2 epitaxy are shown in Fig. 7. The layer / substrate interface is clear and free of cracks and inclusions of other phases. The thickness of the grown layer is uniform over the whole part of the substrate subjected to LPE. For the studied sample, it is measured to be 39±3 μm. The grown Tm^{3+}:CaF_2 film appears darker than its substrate due to the refractive index difference Δn which is estimated to be around 0.06 at 633 nm ($\Delta n = n_{\text{film}} - n_{\text{substrate}}$), according to [16]. Physically, the increase of the film refractive index with Tm^{3+} doping is due to the higher atomic weight of Tm as compared to Ca. There are no cracks propagating through the film. The top surface of the film is not polished and thus appears to be bright because of light scattering.

4.2. Structure of the films

The phase purity, the structure and the orientation of the Tm^{3+}:CaF_2 films were studied by XRD, Fig. 8(a). The measured XRD pattern contains three intense and narrow reflections assigned to the (200), (400) and (600) crystallographic planes of cubic CaF_2 (fluorite, space group O^5_h – $Fm\bar{3}m$, No. 225). Here, (*hkl*) are the Miller's indices. This confirms the good crystallinity of the grown film, as well as its orientation orthogonal to the [100] axis, consistent with the orientation of the substrate. By zooming on each diffraction peak as shown in Fig. 8(b) for the (400) one, we observed that it is splitted in two sub-peaks: one narrow and intense sub-peak at higher diffraction angles 2θ corresponding to the CaF_2 substrate and another broader and weaker one at smaller 2θ angles corresponding to the Tm^{3+}:CaF_2 film. These two sub-peaks are slightly shifted with respect to each other by 2θ less than 0.2°. This is due to the difference of lattice parameter *a* between the CaF_2 substrate and the Tm^{3+}:CaF_2 film.

In cubic CaF_2, the RE^{3+} ions and, in particular, the Tm^{3+} ones are replacing the Ca^{2+} ones. Due to the charge difference between the active ions and the host-forming ones, a charge compensation mechanism is required. For RE^{3+}:CaF_2 grown under oxygen-free conditions, the charge neutrality is maintained due to interstitial fluorine anions F_i^- [29,33] according to a chemical formula $Ca_{1-x}RE_xF_{2+x}$ [34]. The predominant dipolar complex is that with a tetragonal (C_{4v}) symmetry in which F_i^- occupies a nearest-neighbor (NN) interstitial site. Many other configurations, e.g., those with O_h or C_{3v} symmetries, or even cluster sites for moderate and high RE^{3+} concentrations, may appear. This leads to a variety of spectroscopic sites for the RE^{3+} ions and, thus, to broadened absorption and emission bands (a glassy-like behavior). To decrease the variety of RE^{3+} sites, the RE^{3+}:CaF_2 crystals can be intentionally codoped by univalent alkali cations (Na^+, Li^+, K^+) [35-37] acting as charge compensators and introduced in the growth charge in the form of NaF, LiF or KF. Such cations can have substitutional (replacing the Ca^{2+} ions) or interstitial positions near the RE^{3+} ions [38] efficiently forming the RE^{3+}-Na^+(Li^+) complexes and thus breaking the RE^{3+} clusters. The first described mechanism (relying on F_i^-) is involved in the case of LPE CaF_2 thin-films grown using the $CaCl_2$ solvent [15,16]. For the CaF_2 thin-films grown using the LiF solvent, both mechanisms may appear.

The lattice parameters of the substrate and the film were respectively calculated by considering all the observed diffraction peaks to be a_{film} = 5.4806 Å and $a_{substrate}$ = 5.4658 Å. The difference of these parameters $\Delta a = a_{substrate} - a_{film}$ is equal to –0.0148 Å, corresponding to a relative lattice mismatch $|\Delta a/a_{substrate}|$ of 0.27%. For the previously studied LPE-grown Tm^{3+}-doped thin crystalline films, even lower $|\Delta a/a_{substrate}|$ values were achieved, down to 0.03% for Tm:$Y_3Al_5O_{12}$/$Y_3Al_5O_{12}$ [10] and 0.05% for Tm:$KY_{1-x-y}Lu_xGd_y$/$KY(WO_4)_2$ [9,12]. The grown Tm^{3+}:CaF_2 film is subjected to an extension strain ($\Delta a < 0$). The experimental value of a_{film} can be compared with the calculated one obtained from the Vegard's law, suggested for $Ca_{1-x}Tm_xF_{2+x}$ solid solutions with a cubic fluorite-type structure by Sobolev and Fedorov [34]. The latter can be applied if the variation of the lattice mismatch with the substitution rate is linear, which is the case of Tm^{3+} ions in CaF_2. In this way, a_{film} was

estimated as $a_{substrate} + 0.144 \cdot X_{Tm}$ (Å) ≈ 5.4744 Å, where X_{Tm} is the actual Tm^{3+} doping level in at.%, which is in a reasonable agreement with the experimental value.

Physically, the increase of the CaF_2 lattice parameter with Tm^{3+} doping can be explained as following. Despite the fact that the ionic radius of Tm^{3+} (1.13 Å for the VIII-fold F^- coordination) is smaller than that of Ca^{2+} (1.26 Å) [39], the introduction of Tm^{3+} ions in CaF_2 involves interstitial F_i^- anions ensuring the charge compensation. Moreover, the tendency for the active ions to form clusters is enhanced by increasing the Tm^{3+} doping concentration (see Section 4.4). Both these factors lead to expansion of the lattice.

The reciprocal space mapping of the (400) node is shown in Fig. 9(a). It leads to the rocking curves for the CaF_2 substrate and the Tm^{3+}:CaF_2 film plotted in Fig. 9(b). The acquisition time for this measurement was 7 h 30 min. The full width at half maximum (FWHM) for the two rocking curves is 0.039° and 0.096°, respectively, which reflects the very low crystalline mosaicity of the film compared to the substrate, estimated to be ±0.03°. In other words, there is a very low local disorientation of the crystalline planes regarding the normal to the surface.

4.3. Composition of the films

The composition of the Tm^{3+}:CaF_2 films was investigated by Energy Dispersive X-ray spectroscopy. At first, a SEM image of the film was captured with a magnification of 100×, Fig. 10. It shows a net-like textured surface in agreement with the optical microscopy observations.

A typical EDX spectrum of the Tm^{3+}:CaF_2 film is shown in Fig. 11, which confirms the presence of host-forming elements (Ca and F) in an atomic ratio close to 1:2, as well as the dopant (Tm). The EDX study reveals the presence of traces of other elements such as O, Al and Si. The weak concentrations of oxygen and silicon are probably due to evaporation from the quartz (SiO_2) chamber. A minor amount of oxygen can also come from an imperfect sealing of the growth chamber and/or the airlock during the samples exchange. The weak Al pollution is probably due to impurities existing in the CaF_2 reagent. With the used EDX detector, it was not possible to detect such light elements like Li.

Furthermore, a 2D element mapping based on EDX measurements was performed. The results for the Ca, F and Tm elements are shown in Fig. 12 and compared with the corresponding SEM image of the analyzed area. The distribution of calcium and fluorine is following the hilly morphology of the as-grown surface. The Tm^{3+} ions are uniformly distributed in the film suggesting its good suitability for further spectroscopic studies.

The actual Tm^{3+} doping concentration averaged over a large film area was estimated from transmission measurements using the previously reported absorption cross-sections of Tm^{3+} ions in CaF_2 [29] and the measured thickness of the films to be 6.0±0.5 at.% (with respect to Ca). Thus, the segregation coefficient for Tm^{3+} ions, $K_{Tm} = X_{Tm}(film)/X_{Tm}(batch)$ is ~0.4. Note that for bulk Tm^{3+}:CaF_2 crystals, this parameter is typically close to the unity, e.g., K_{Tm} = 1.05 [40]. For the recently studied Yb^{3+}:CaF_2 LPE films grown by using the $CaCl_2$ solvent, the Yb^{3+} segregation coefficient was also below the unity [41] which agrees with the results of the present work. The possible reason for less than unity segregation coefficients K_{RE}

achieved in the LPE experiments is that the growth temperature in this case is much lower than during the growth of bulk crystals.

4.4. Luminescence of thulium ions

The luminescence spectrum of Tm^{3+} ions in the CaF_2 LPE layers is shown in Fig. 13. The emission corresponds to the $^3F_4 \rightarrow {}^3H_6$ transition. The emission band is broad and smooth and it spans from 1.55 to 2.15 μm.

It is known that the RE^{3+} ions exhibit strong clustering effect in CaF_2, when the doping concentration is exceeding about 0.1 at.% [29,33]. In the cubic structure of CaF_2, the F^- anions are located at the corners of the lattice cubes. Half of these cubes are occupied by the Ca^{2+} cations while the other half is empty. The RE^{3+} ions substitute the Ca^{2+} ones, so that a charge compensation is required, as previously noticed. For low Tm^{3+} concentrations, depending on the way that the charge compensation occurs, there exists three main types of isolated sites for Tm^{3+} ions with a different local symmetry (cubic – O_h, tetragonal – C_{4v} or trigonal – C_{3v}) [29] and each of these Tm^{3+} ion sites presents a typical luminescence spectrum. For higher Tm^{3+} concentrations, the fluorescence spectra are mostly determined by the emission of Tm^{3+} clusters.

For comparison, we have measured the luminescence spectra of several bulk Tm^{3+}:CaF_2 crystals doped with 0.1, 0.5 and 4.7 at.% Tm^{3+}, as shown in Fig. 13. For the crystal with the lowest Tm^{3+} doping (containing predominantly isolated ions), the spectrum exhibits two distinct emission peaks in the short-wavelength part centered at 1605 and 1663 nm. The FWHM of the whole spectrum is 157 nm. The crystal with the highest studied Tm^{3+} doping (for which the clustering is already strong), exhibits red-shifted peaks at 1612 and 1668 nm and a slightly narrower spectrum (FWHM = 147 nm) indicating the crystal-field change.

The luminescence spectrum of the Tm^{3+}:CaF_2 film is similar to that obtained for highly doped bulk crystal but it is broader (FWHM = 180 nm). This indicates that Tm^{3+} clusters are likely formed in the film while the exact nature of the luminescent centers needs to be further clarified by low-temperature spectroscopy or high-resolution transmission electron microscopy (HRTEM) [42]. Regarding the predominant charge compensation mechanism (cf. Section 4.2), it seems that the interstitial F_i^- anions play a key role in formation of the cluster sites. Indeed, in the presence of Li^+, the Tm^{3+} clusters would be efficiently broken which is not observed in Fig. 13.

In our previous study of the Yb^{3+}:CaF_2 film grown by the LPE method using $CaCl_2$ as a solvent, a key role of oxygen-assisted sites in the Yb^{3+} luminescence was revealed [41]. To identify their possible effect on the grown Tm^{3+}:CaF_2 film, we have also studied a bulk Tm^{3+}:CaF_2 crystal with an oxyfluoride phase (i.e., grown in an oxygen enriched atmosphere), see Fig. 13. The measured spectrum is clearly different from that of the Tm^{3+}:CaF_2 film, suggesting that the fraction of Tm^{3+} ions in oxygen-assisted sites is rather low.

The broadband emission behavior of Tm^{3+} ions and the positive refractive index contrast between the film and the substrate indicate the high suitability of Tm^{3+}:CaF_2 thin films for waveguide laser operation. Obviously, to ensure this, the top surface of the film should be additionally polished to reduce the waveguide propagation losses.

5. Conclusions

We demonstrate for the first time the suitability of the binary system CaF_2-LiF (with CaF_2 / LiF acting as a solute / solvent, respectively) for the Liquid Phase Epitaxy of single-crystalline rare-earth-doped CaF_2 thin films. The LiF solvent is not corrosive and it allows to obtain crack-free thin films with a good reproducibility in a broad range of growth temperatures.

Crystalline thin films of ~6 at.% Tm^{3+}:CaF_2 with a thickness of 20–120 μm were grown onto (100) oriented undoped bulk CaF_2 substrates with growth rates of 0.5–2.0 μm/min, depending on the growth temperature (853–865 °C) and duration (20–60 min). The as-grown films exhibited low RMS surface roughness of about 1 μm, uniform thickness and very low mosaicity as confirmed by confocal microscopy, XRD and SEM. The Tm^{3+} ions were uniformly distributed in the films, according to the EDX-based elementary mapping. Moderate to high Tm^{3+} doping concentrations are accessible in the films which is attractive for laser applications. The films exhibit broadband Tm^{3+} luminescence at ~2 μm which is probably assigned to Tm^{3+} clusters and the emission bandwidth for the films is slightly broader than that for corresponding bulk crystals.

The proposed LPE growth approach based on selecting LiF as a solvent, together with the good thermal properties of CaF_2, are promising for further laser applications of RE^{3+}-doped CaF_2 thin films.

Acknowledgements

The authors acknowledge the French Research National Agency (ANR) through the LabEx EMC3 project FAST-MIR, the European Community funds FEDER and the Normandie region, for their financial support and funding.

References

1. B. Ferrand, B. Chambaz, M. Couchaud, Opt. Mater. 11 (1999) 101.
2. S.L. Blank, J.W. Nielsen, J. Cryst. Growth 17 (1972) 302.
3. P.K. Tien, R.J. Martin, S.L. Blank, S.H. Wemple, L.J. Varnerin, Appl. Phys. Lett. 21 (1972) 207.
4. J.G. Grabmaier, R.D. Plätner, P. Möckel, W.W. Krühler, J. Cryst. Growth 34 (1976) 280.
5. F. Starecki, W. Bolaños, G. Brasse, A. Benayad, M. Morales, J-L. Doualan, A. Braud, R. Moncorgé, P. Camy, J. Cryst. Growth 401 (2014) 537.
6. W. Bolanos, J.J. Carvajal, M.C. Pujol, X. Mateos, G. Lifante, M. Aguiló, F. Díaz, Cryst. Growth Design 9 (2009) 3525.
7. D. Pelenc, B. Chambaz, I. Chartier, B. Ferrand, C. Wyon, D.P. Shepherd, D.C. Hanna, A.C. Large, A.C. Tropper, Opt. Commun. 115 (1995) 491.
8. P. Loiko, R. Soulard, G. Brasse, J.-L. Doulan, B. Guichardaz, A. Braud, A. Tyazhev, A. Hideur, P. Camy, Opt. Express 26 (2018) 24653.

9. S. Aravazhi, D. Geskus, K. van Dalfsen, S.A. Vázquez-Córdova, C. Grivas, U. Griebner, S.M. García-Blanco, M. Pollnau, Appl. Phys. B 111 (2013) 433.
10. A. Rameix, C. Borel, B. Chambaz, B. Ferrand, D. P. Shepherd, T. J. Warburton, D. C. Hanna, A. C. Tropper, Opt. Commun. 142 (1997) 239.
11. W. Bolanos, F. Starecki, A. Benayad, G. Brasse, V. Ménard, J.-L. Doualan, A. Braud, R. Moncorgé, P. Camy, Opt. Lett. 37 (2012) 4032.
12. K. van Dalfsen, S. Aravazhi, D. Geskus, K. Wörhoff, M. Pollnau, Opt. Express 19 (2011) 5277.
13. E. Molva, Opt. Mater. 11 (1999) 289.
14. X. Mateos, S. Lamrini, K. Scholle, P. Fuhrberg, S. Vatnik, P. Loiko, I. Vedin, M. Aguiló, F. Díaz, U. Griebner, V. Petrov, Opt. Lett. 42 (2017) 3490.
15. A. Peña, P. Camy, A. Benayad, J.-L. Doualan, C. Maurel, M. Olivier, V. Nazabal, R. Moncorgé, Opt. Mater. 33 (2011) 1616.
16. S. Renard, P. Camy, J. L. Doualan, R. Moncorgé, M. Couchaud, B. Ferrand, Opt. Mater. 28 (2006) 1289.
17. I. H. Malitson, Appl. Opt. 2 (1963) 1103.
18. G.A. Slack, Phys. Rev. 122 (1961) 1451.
19. F. Druon, S. Ricaud, D. N. Papadopoulos, A. Pellegrina, P. Camy, J. L. Doualan, R. Moncorgé, A. Courjaud, E. Mottay, P. Georges, Opt. Mater. Express 1 (2011) 489.
20. P. Camy, J.L. Doualan, S. Renard, A. Braud, V. Menard, R. Moncorgé, Opt. Commun. 236 (2004) 395.
21. K. Nassau, J. Appl. Phys. 32 (1961) 1820.
22. L.J. Schowalter, R.W. Fathauer, J. Vac. Sci. Technol. A 4 (1986) 1026.
23. N. Mattoso, D.H. Mosca, W.H. Schreiner, I. Mazzaro, S.R. Teixeira, Thin Solid Films 272 (1996) 83.
24. J.K. Ko, J.H. Park, S.W. Choi, S.H. Park, J. Yi, Thin Solid Films 427 (2003) 259.
25. J.G. Cook, G.H. Yousefi, S.R. Das, D.F. Mitchell, Thin Solid Films 217 (1992) 87.
26. T. Maki, K. Okamoto, M. Sugiura, T. Hosomi, T. Kobayashi, Appl. Surf. Sci. 197 (2002) 448.
27. L.E. Bausa, G. Lifante, E. Daran, P.L. Pernas, Appl. Phys. Lett. 68 (1996) 3242.
28. F. Lahoz, E. Daran, G. Lifante, T. Balaji, A. Muñoz-Yagüe, Appl. Phys. Lett. 74 (1999) 1060.
29. T. Balaji, G. Lifante, E. Daran, R. Legros, G. Lacoste, Thin Solid Films 339 (1999) 187.
28. K. Scholle, S. Lamrini, P. Koopmann, and P. Fuhrberg, in Frontiers in Guided Wave Optics and Optoelectronics, B. Pal, Ed. (InTech, 2010), pp. 471–500.
29. S. Renard, P. Camy, A. Braud, J.L. Doualan, R. Moncorgé, J. Alloy Compd. 451 (2008) 71.
30. W.E. Roake, J. Electrochem. Soc. 104 (1957) 661.
31. M.L. Falin, K.I. Gerasimov, V.A. Latypov, A.M. Leushin, H. Bill, D. Lovy, J. Lumin. 102-103 (2003) 239.
32. A. Boulle, J. Appl. Cryst. 50 (2017) 967.

33. V. Petit, P. Camy, J-L. Doualan, X. Portier, R. Moncorgé, Phys. Rev. B 78 (2008) 085131.
34. B.P. Sobolev, P.P. Fedorov, J. Less-Common Met. 60 (1978) 33.
35. L. Su, J. Xu, H. Li, W. Yang, Z. Zhao, J. Si, Y. Dong, and G. Zhou, Opt. Lett. 30 (2005) 1003.
36. S. Hraiech, A. Jouini, K.J. Kim, Y. Guyot, A. Yoshikawa, G. Boulon, Radiat. Measur. 45 (2010) 323-327.
37. G.D. Jones, R.J. Reeves, J. Lumin. 87 (2000) 1108-1111.
38. I. Nicoara, M. Stef, Eur. Phys. J. B 85 (2012) 180.
39. A.A. Kaminskii, Laser crystals: their physics and properties (Springer, 2013).
40. X. Guo, J. Wang, D. Jiang, X. Qian, C. Zhang, Y. Zu, J. Liu, B. Mei, L. Su, Opt. Commun. 435 (2019) 5.
41. P. Loiko, R. Soulard, E. Kifle, L. Guillemot, G. Brasse, A. Benayad, J.-L. Doulan, A. Braud, M. Aguiló, F. Díaz, X. Mateos, P. Camy, Opt. Express 27 (2019) 12647.
42. B. Lacroix, C. Genevois, J. L. Doualan, G. Brasse, A. Braud, P. Ruterana, P. Camy, E. Talbot, R. Moncorge and J. Margerie, J. Phys. Rev. B 90 (2014) 125124.

List of figure captions

Fig. 1. Phase diagram of the binary CaF_2-LiF system, (s) stands for solid phase.

Fig. 2. Experimental set-up for Liquid Phase Epitaxy growth of Tm^{3+}:CaF_2 thin-films on undoped CaF_2 substrates.

Fig. 3. Scheme of fabrication of single-crystalline Tm^{3+}:CaF_2 thin films on (100)-oriented undoped CaF_2 substrates. Cz – Czochralski growth method.

Fig. 4. Observation of the raw surface (top view) of an LPE grown Tm^{3+}:CaF_2 film using a confocal optical microscope in the bright-field: the objective magnification is (a) ×10 and (b) ×100, λ = 405 nm.

Fig. 5. Observation of the raw surface (top view) of an LPE grown Tm^{3+}:CaF_2 film using a confocal optical microscope in the bright-field: the objective magnification is (a) ×10 and (b) ×100, λ = 405 nm.

Fig. 6. Surface roughness plot for the as-grown Tm^{3+}:CaF_2 LPE film: *blue lines* indicate the range of root-mean-square (RMS) deviation of the roughness, *arrows* indicate positions of the hills and valleys; *inset* shows the corresponding topography map measured using a confocal optical microscope, A-B is the analyzed direction, λ = 405 nm.

Fig. 7. (a,b) Optical microscope images of the polished end-facet of the Tm^{3+}:CaF_2 / CaF_2 epitaxy.

Fig. 8. (a,b) High resolution X-ray diffraction (XRD) patterns for the Tm^{3+}:CaF_2 / CaF_2 epitaxy: (a) the range of the diffraction angles 2θ = 20–120°, (b) a detailed view on the (400) reflection; (hkl) are the Miller's indices for cubic CaF_2. *Blue vertical lines* in (a) – theoretical peaks for bulk powder CaF_2.

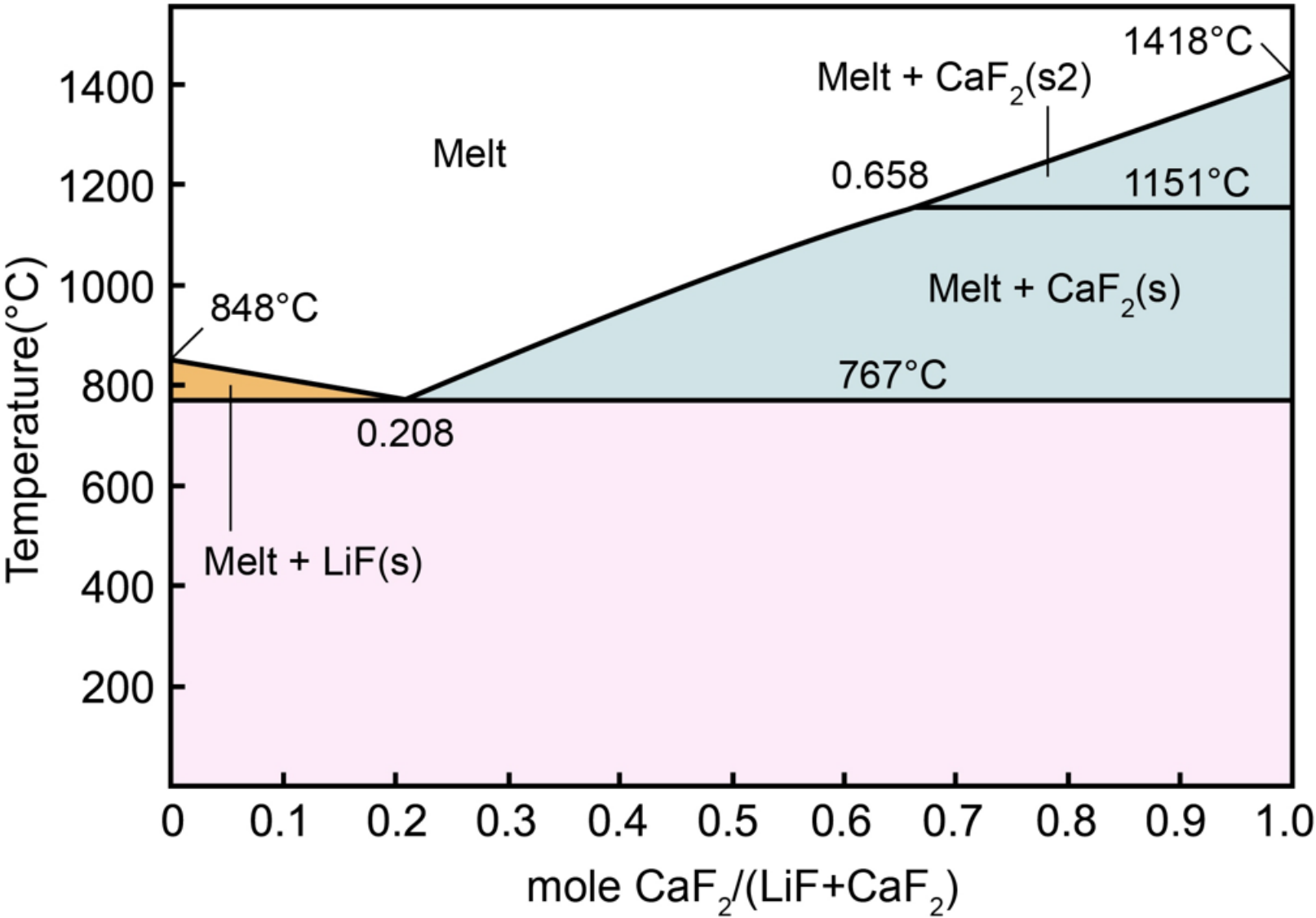
Fig. 9. (a) Reciprocal space mapping of the (400) node for the Tm^{3+}:CaF_2 / CaF_2 epitaxy; (b) rocking curve of the (400) node of the LPE Tm^{3+}:CaF_2 film.

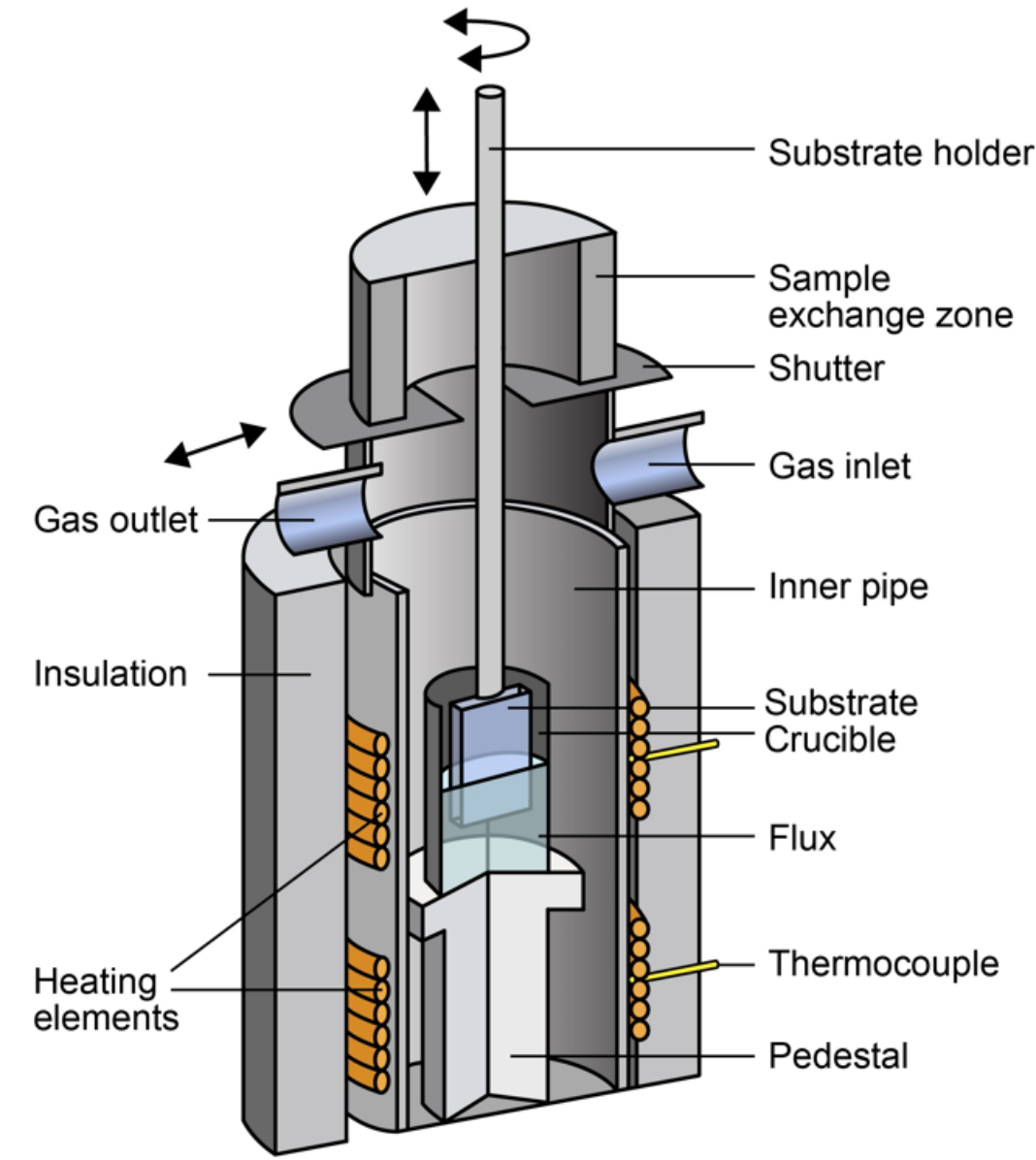
Fig. 10. Scanning Electron Microscope (SEM) image of the raw surface (top view) of an LPE grown Tm^{3+}:CaF_2 film. The magnification is 100x.

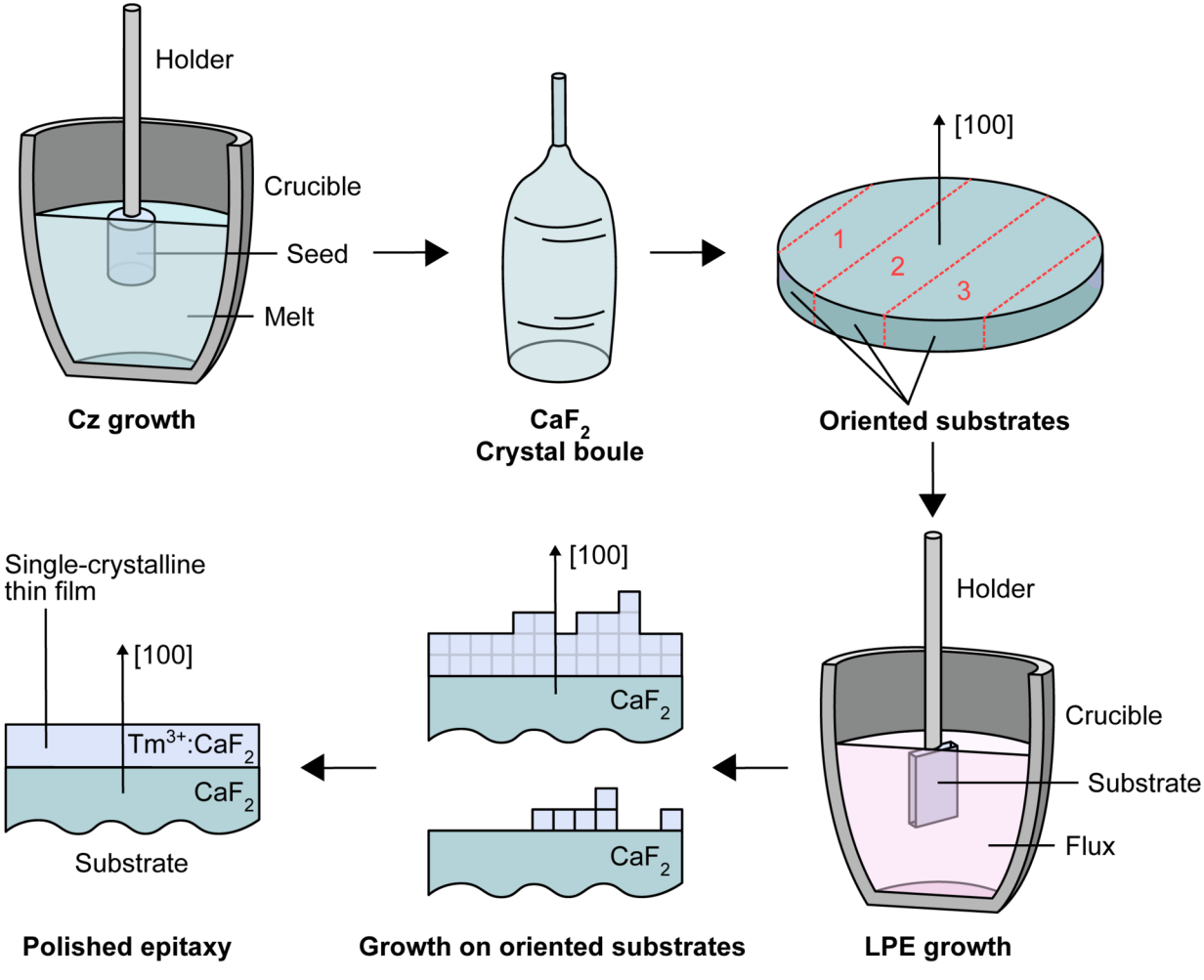
Fig. 11. Typical EDX spectrum of the LPE grown Tm^{3+}:CaF_2 film.

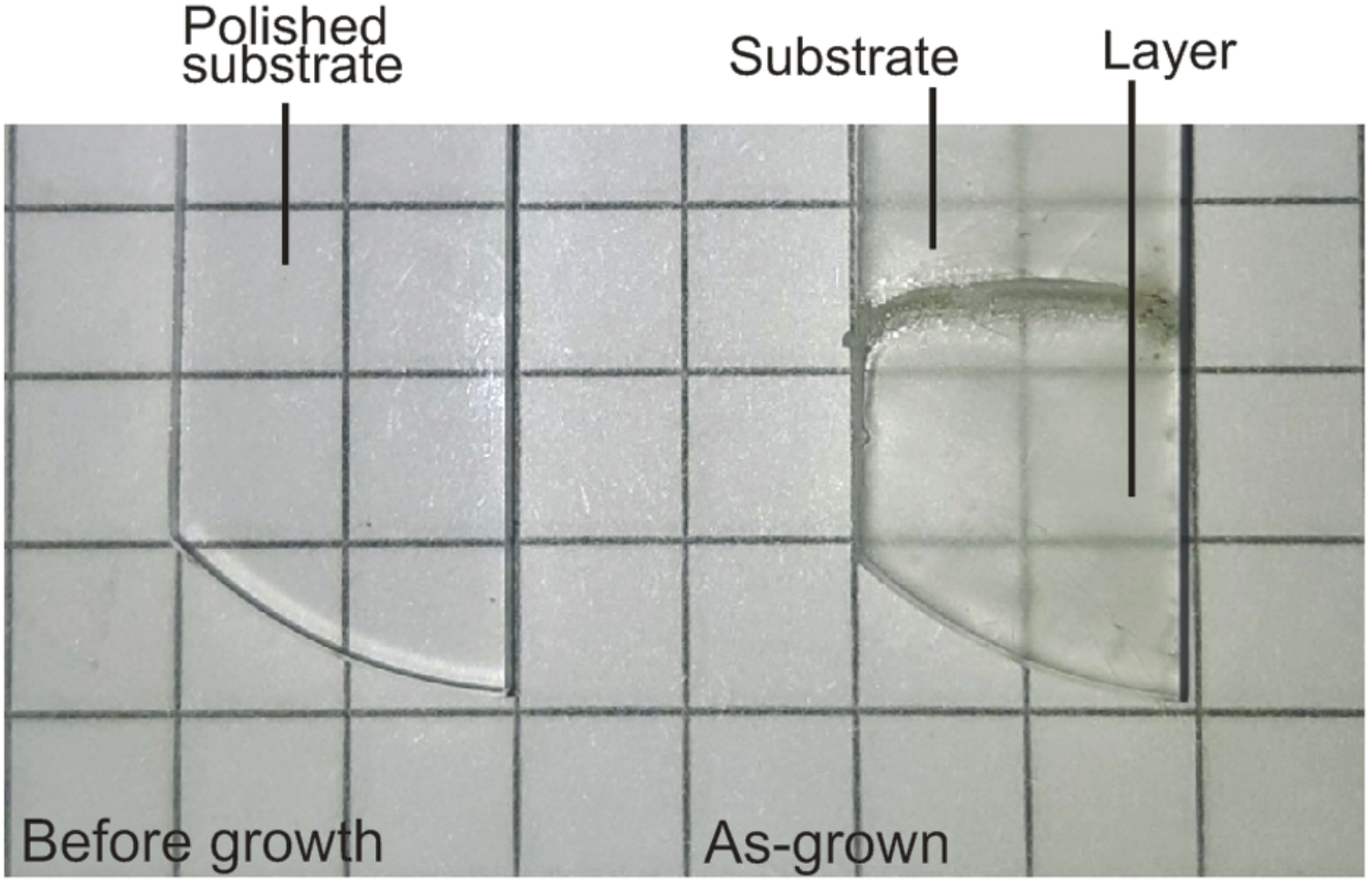
Fig. 12. (a) SEM image and (b-d) the corresponding EDX element mapping of the LPE grown Tm^{3+}:CaF_2 film: (b) Ca Kα1 line, (c) F Kα1,2 lines, (d) Tm Lα1 line. Brighter colors represent higher element amounts.

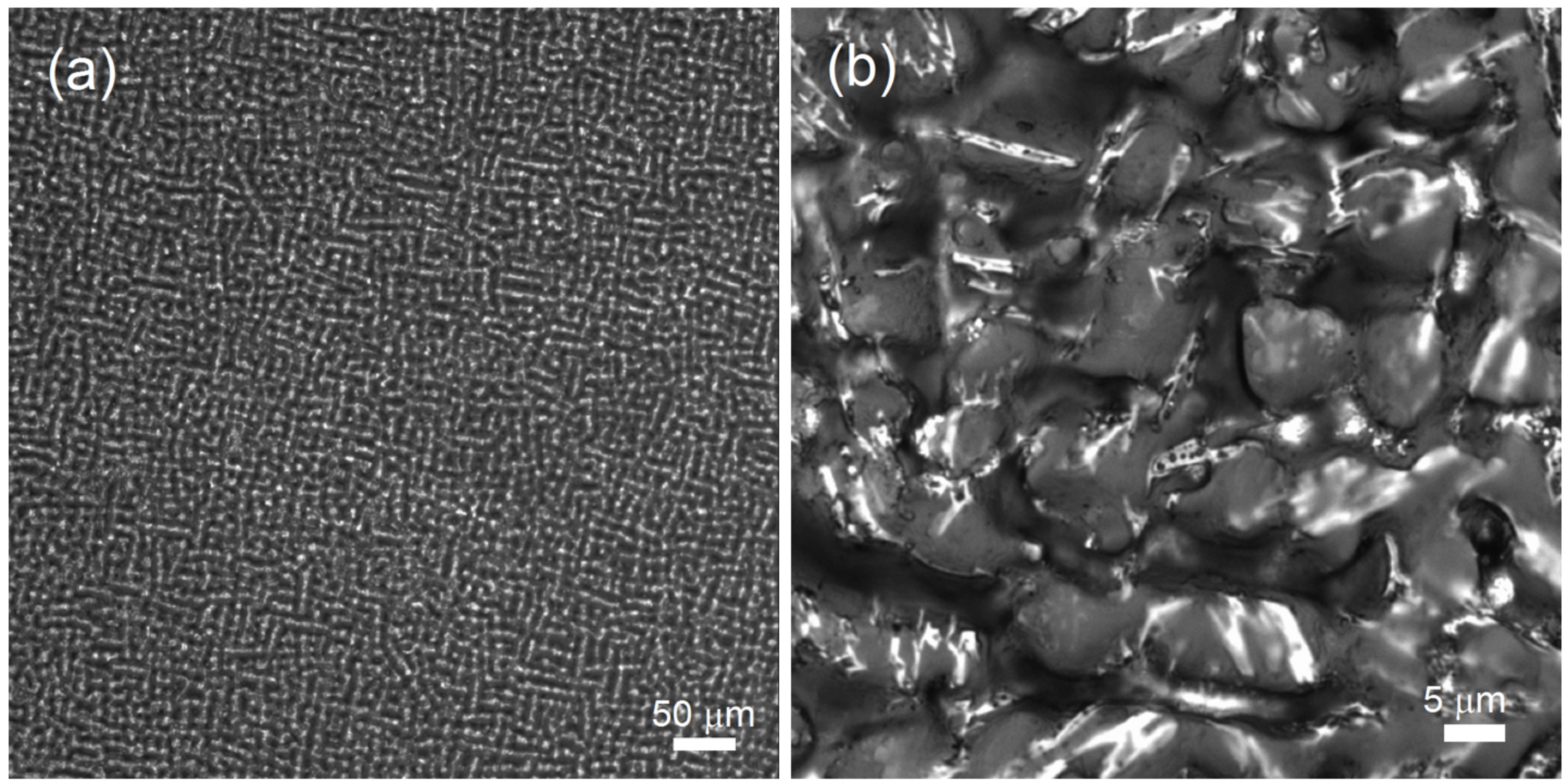
Fig. 13. Luminescence spectrum of Tm^{3+} ions in the LPE grown ~6 at.% Tm^{3+}:CaF_2 layers ($^3F_4 \rightarrow {}^3H_6$ transition). The spectra for bulk Tm^{3+}:CaF_2 crystals with different Tm^{3+} doping levels, as well as with a presence of the oxyfluoride phase are given for comparison. The excitation wavelength is 765 nm.

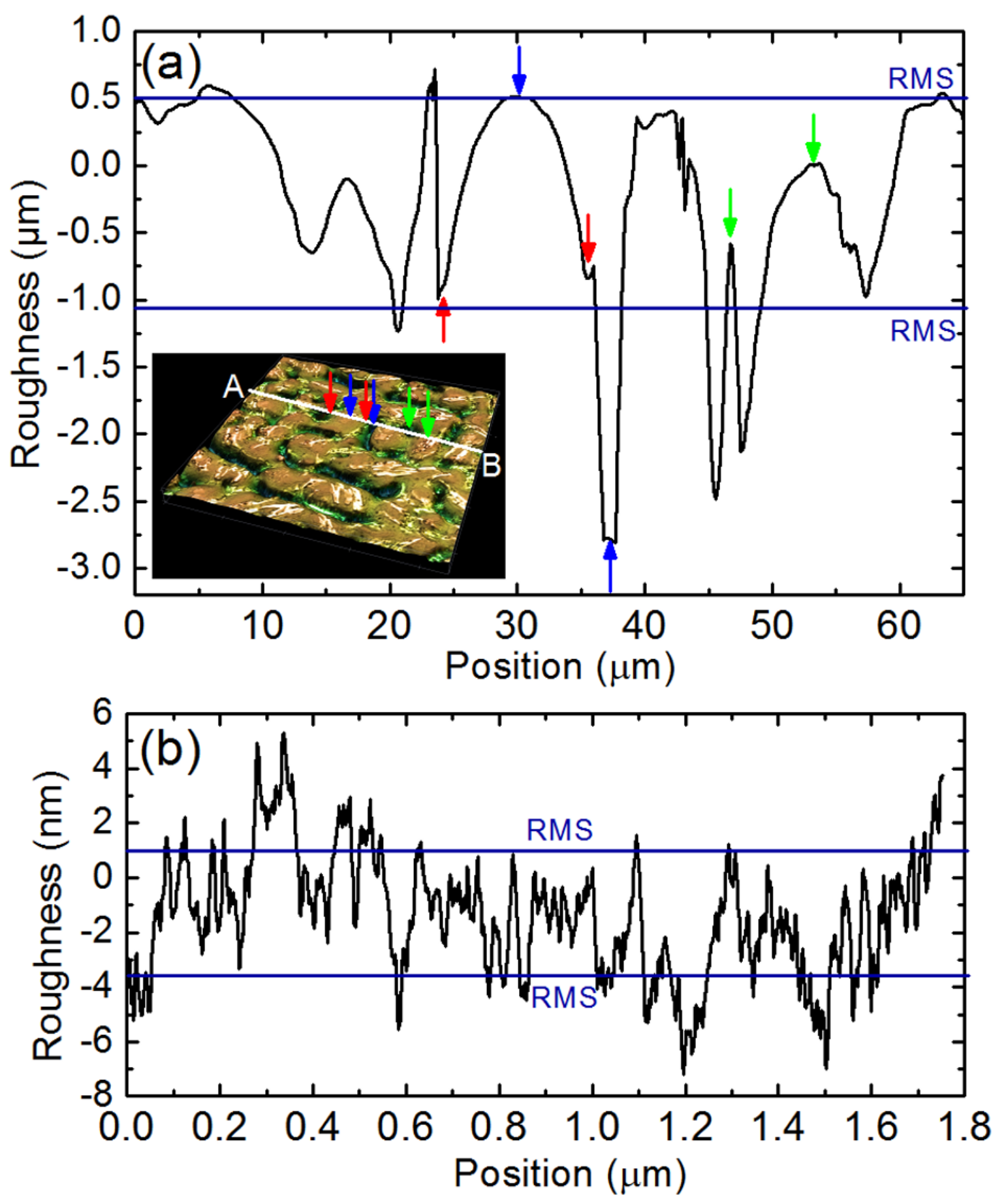

1418°C
Melt + CaF2(s2)
Melt
0.658
1151°C
Melt + CaF2(s)
848°C
767°C
0.208
Melt + LiF(s)
Temperature(°C)
1400
1200
1000
800
600
400
200
0
0.1
0.2
0.3
0.4
0.5
0.6
0.7
0.8
0.9
1.0
mole CaF2/(LiF+CaF2)

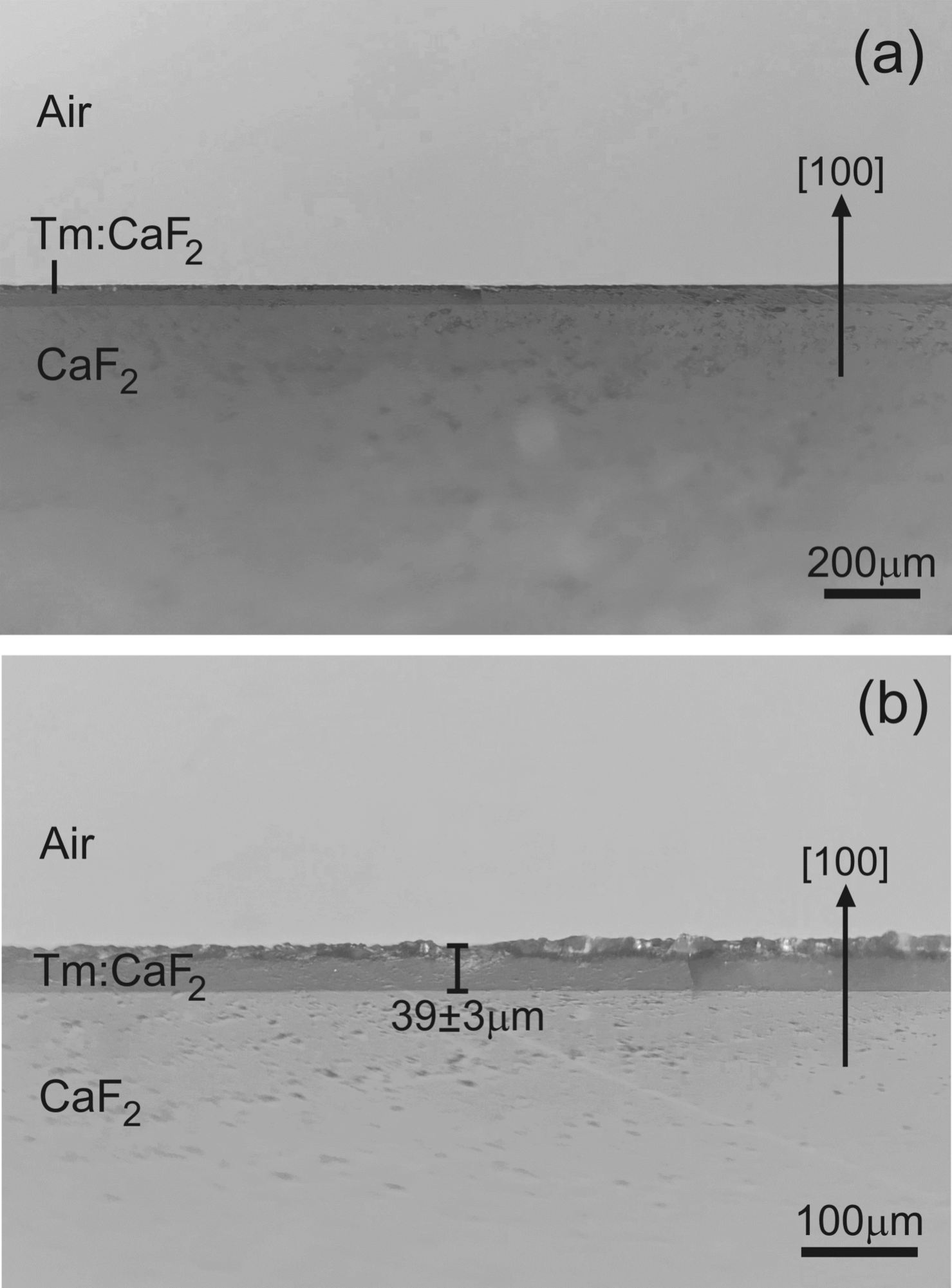

Substrate holder
Sample exchange zone
Shutter
Gas inlet
Gas outlet
Inner pipe
Insulation
Substrate
Crucible
Flux
Thermocouple
Heating elements
Pedestal

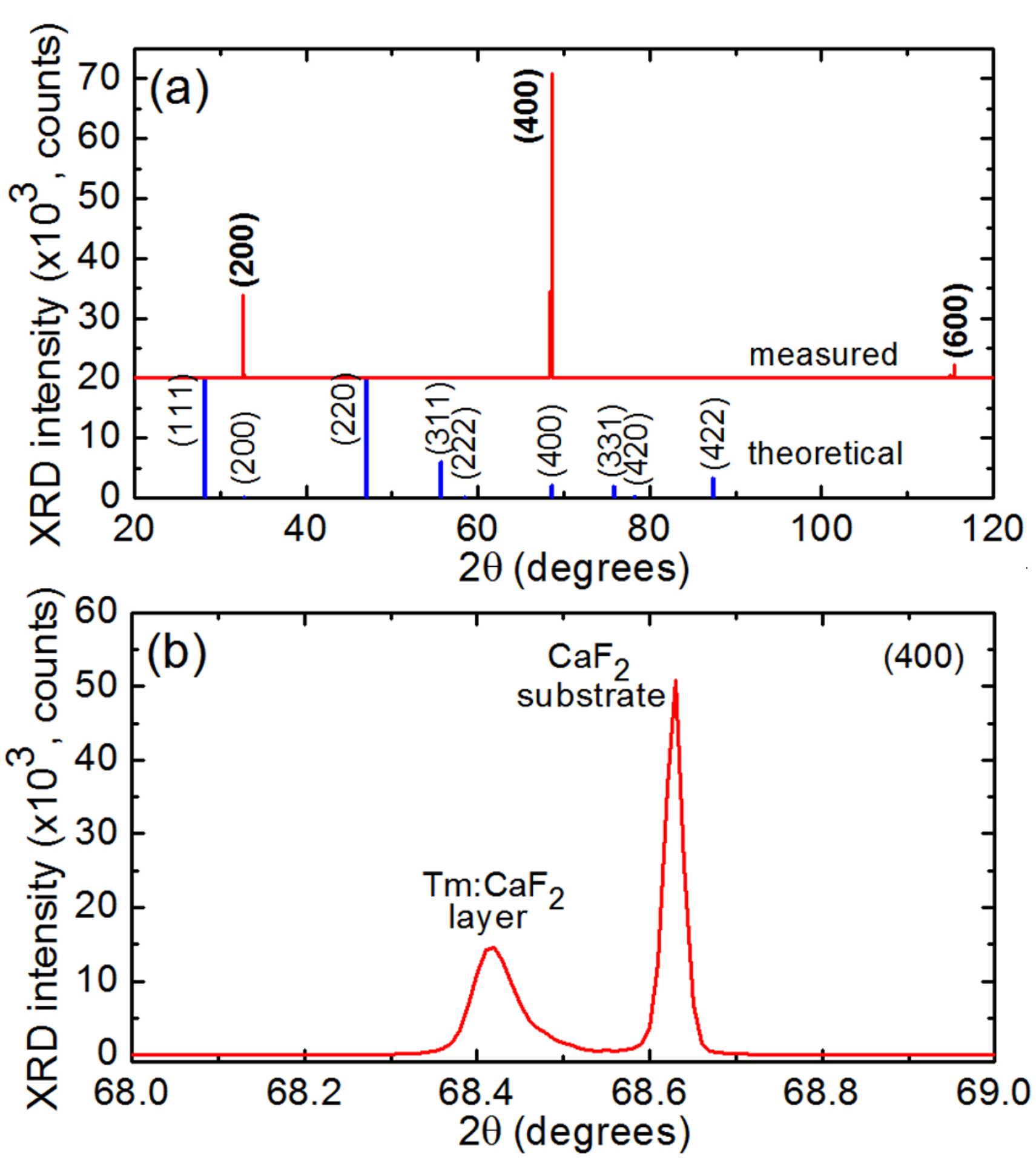

Holder
Crucible
Seed
Melt
Cz growth
CaF2
Crystal boule
[100]
1
2
3
Oriented substrates
Holder
Crucible
Substrate
Flux
LPE growth
[100]
CaF2
CaF2
Growth on oriented substrates
Single-crystalline
thin film
[100]
Tm3+:CaF2
CaF2
Substrate
Polished epitaxy

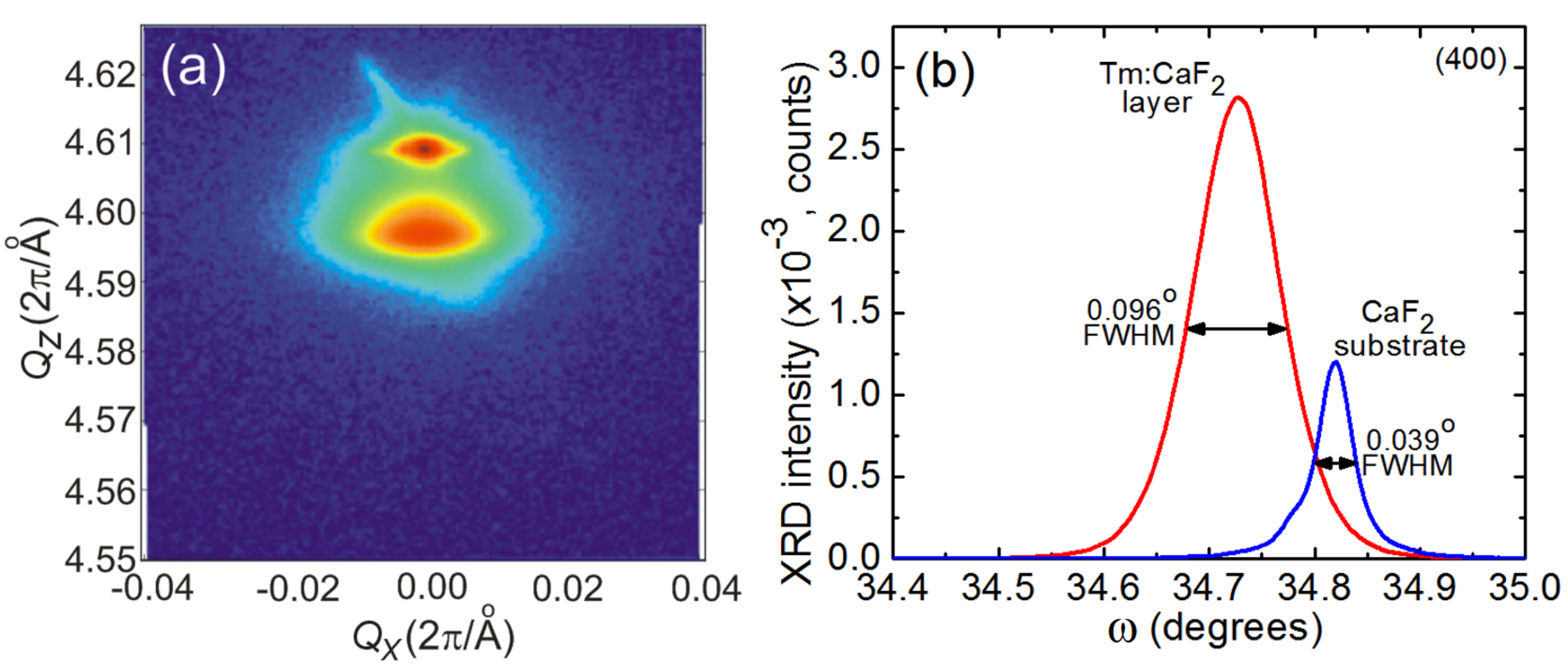

Polished substrate
Substrate
Layer
Before growth
As-grown


(a)
50 μm
(b)
5 μm


(a)
RMS
RMS
A
B
Roughness (μm)
Position (μm)
(b)
RMS
RMS
Roughness (nm)
Position (μm)


(a)
Air
[100]
Tm:CaF2
CaF2
200μm
(b)
Air
[100]
Tm:CaF2
39±3μm
CaF2
100μm


(a)
XRD intensity (x10^3, counts)
2θ (degrees)
(400)
(200)
(600)
measured
theoretical
(111)
(200)
(220)
(311)
(222)
(400)
(331)
(420)
(422)
(b)
CaF2 substrate
(400)
Tm:CaF2 layer
XRD intensity (x10^3, counts)
2θ (degrees)


(a)
4.62
4.61
4.60
4.59
4.58
4.57
4.56
4.55
$Q_Z(2\pi/\text{Å})$
-0.04
-0.02
0.00
0.02
0.04
$Q_X(2\pi/\text{Å})$
(b)
(400)
Tm:CaF_2 layer
0.096° FWHM
CaF_2 substrate
0.039° FWHM
XRD intensity ($x10^{-3}$, counts)
3.0
2.5
2.0
1.5
1.0
0.5
0.0
34.4
34.5
34.6
34.7
34.8
34.9
35.0
ω (degrees)

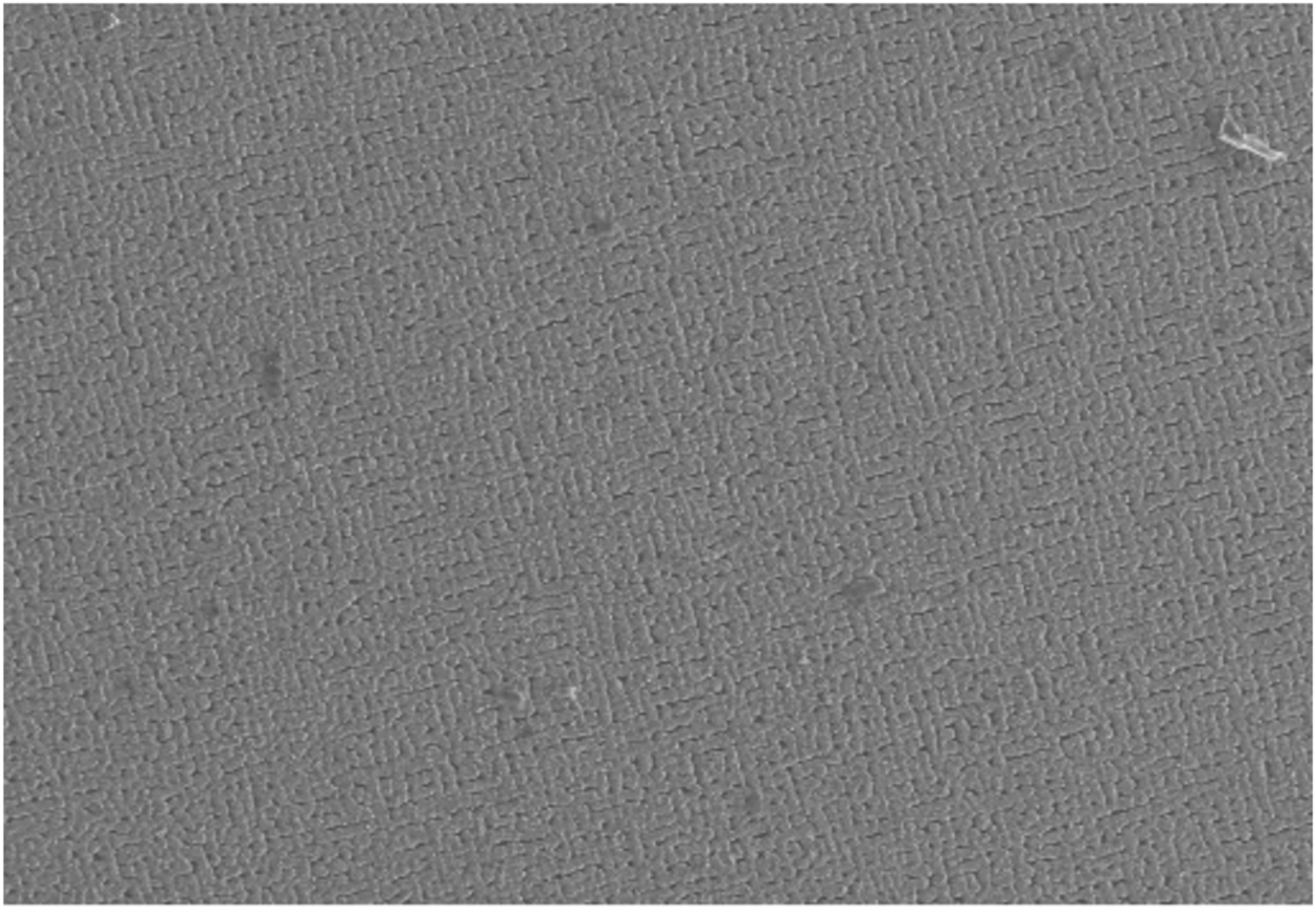
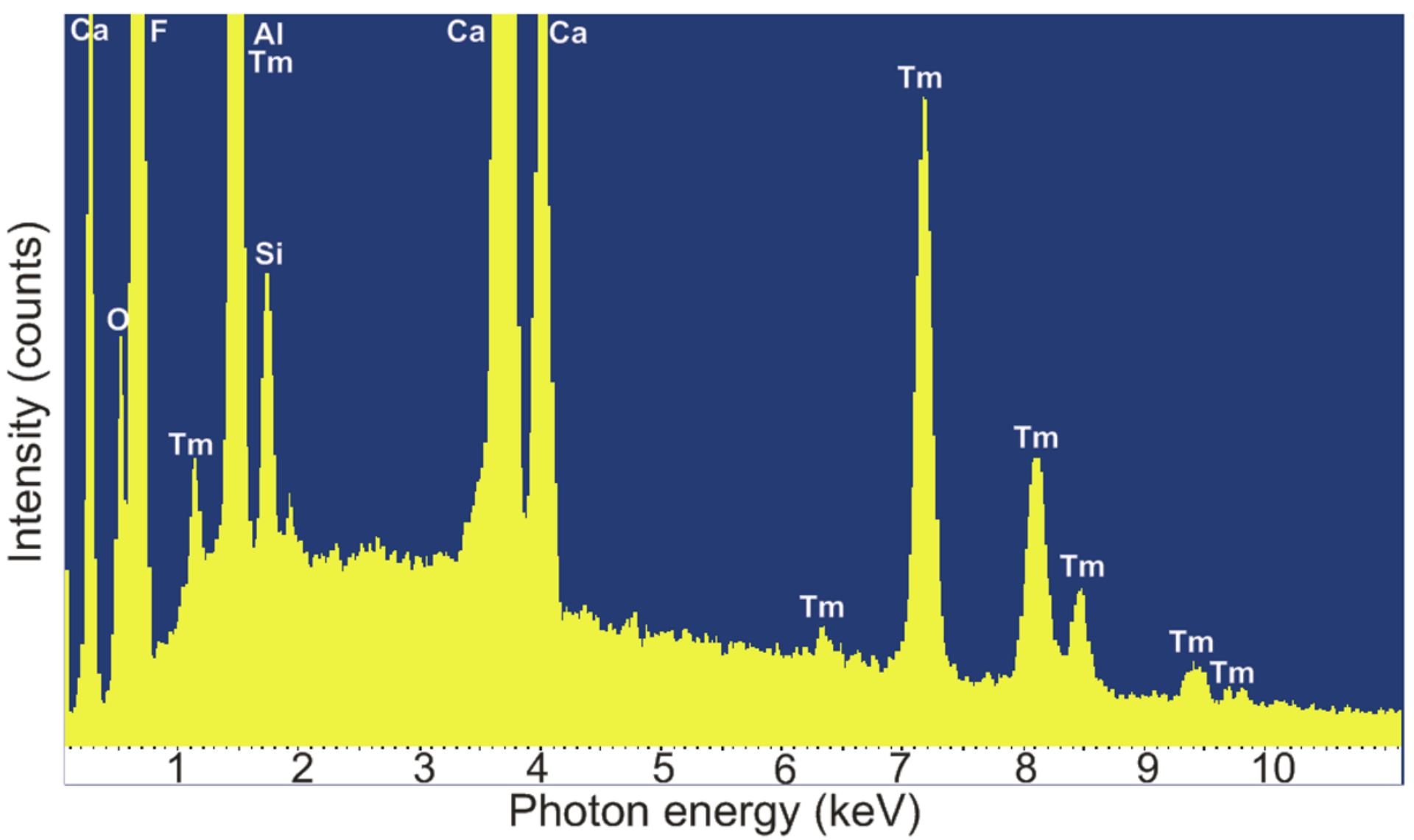
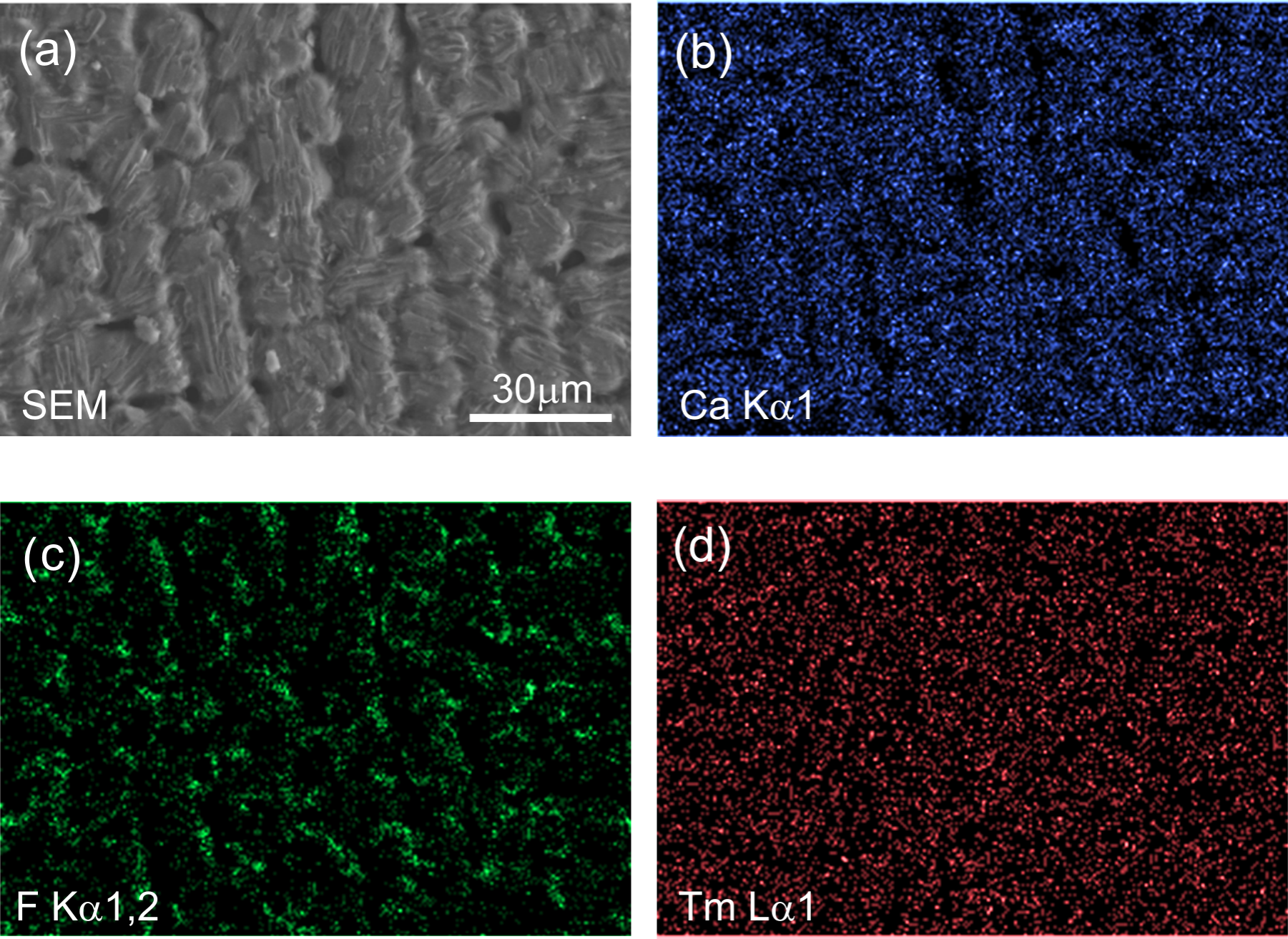
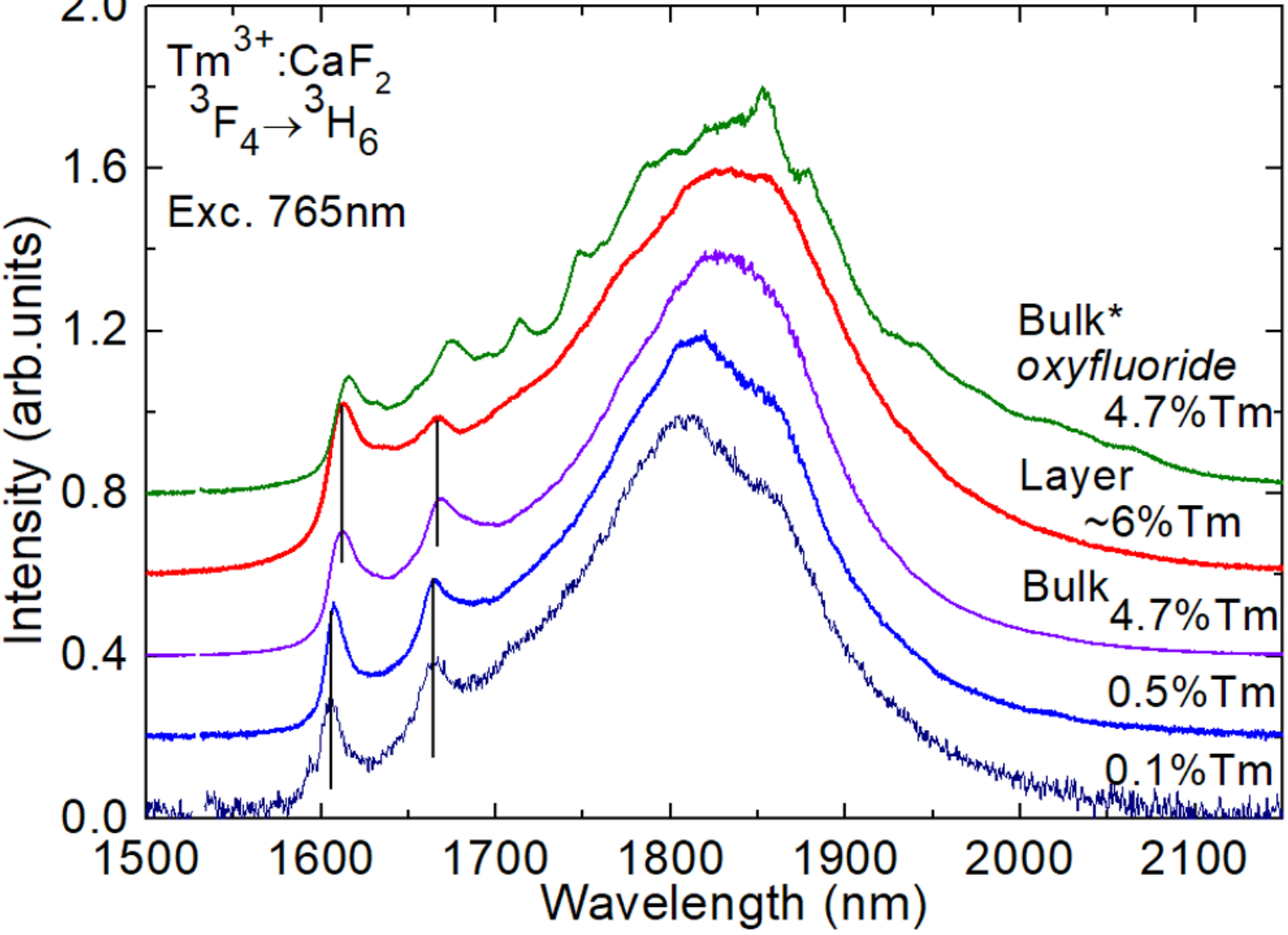


Image électronique 1


Ca
F
Al
Tm
Ca
Ca
Tm
Si
O
Tm
Tm
Tm
Tm
Tm
Tm
Tm
Intensity (counts)
1
2
3
4
5
6
7
8
9
10
Photon energy (keV)


(a)
SEM
30μm
(b)
Ca Kα1
(c)
F Kα1,2
(d)
Tm Lα1


Tm3+:CaF2
3F4→3H6
Exc. 765nm
Bulk*
oxyfluoride
4.7%Tm
Layer
~6%Tm
Bulk
4.7%Tm
0.5%Tm
0.1%Tm
Intensity (arb.units)
Wavelength (nm)
0.0
0.4
0.8
1.2
1.6
2.0
1500
1600
1700
1800
1900
2000
2100